Point-to-point overlay of a 100Gb/s DP-QPSK channel in LR-PONs for urban and rural areas

STEFANO PORTO,[1,*] DANIEL CAREY,[1] NICOLA BRANDONISIO,[1] ALAN NAUGHTON,[1] CLEITUS ANTONY,[1] PETER OSSIEUR,[1] NICK PARSONS,[2] GIUSEPPE TALLI,[1] AND PAUL D. TOWNSEND[1]

[1]*Tyndall National Institute, University College Cork, Cork, Ireland*
[2]*Polatis Ltd., Cambridge, UK*
*stefano.porto@tyndall.ie

Abstract: The continuing growth in information demand from fixed and mobile end-users, coupled with the need to deliver this content in an economically viable manner, is driving new innovations in access networks. In particular, it is becoming increasingly important to find new ways to enable the coexistence of heterogeneous services types which may require different signal modulation formats over the same fiber infrastructure. For example, the same physical layer can potentially be used to deliver shared 10Gb/s services to residential customers, dedicated point-to-point (P2P) 100Gb/s services to business customers, and wireless fronthaul, in a highly cost-effective manner. In this converged scenario, the performance of phase modulated signals can be heavily affected by nonlinear crosstalk from co-propagating on-off-keying (OOK) channels. In this paper, the overlay of a 100G P2P dual-polarization quadrature phase-shift keying (DP-QPSK) channel in a long-reach passive optical network (LR-PON) in the presence of co-propagating 10Gb/s OOK neighboring channels is studied for two different PON topologies. The first LR-PON topology is particularly suited for densely populated areas while the second is aimed at rural, sparsely populated areas. The experimental results indicate that with an emulated load of 40 channels the urban architecture can support up to 100km span and 512 users, while the rural architecture can support up to 120km span and 1024 users. Finally, a system model is developed to predict the system performance and system margins for configurations different from the experimental setups and to carry out design optimization that could in principle lead to even more efficient and robust schemes.

References and links

1. D. Nesset, "NG-PON2 Technology and Standards," J. Lightwave Technol. **33**(5), 1136–1143 (2015).
2. V. Houtsma and D. van Veen, "A Study of Options for High-Speed TDM-PON Beyond 10G," J. Lightwave Technol. **35**(4), 1059–1066 (2017).
3. D. Nesset, "PON Roadmap [Invited]," J. Opt. Commun. Netw. **9**(1), A71–A76 (2017).
4. H. Rohde, E. Gottwald, S. Rosner, E. Weis, P. Wagner, Y. Babenko, D. Fritzsche, and H. Chaouch, "Trials of a Coherent UDWDM PON Over Field-Deployed Fiber: Real-Time LTE Backhauling, Legacy and 100G Coexistence," J. Lightwave Technol. **33**(8), 1644–1649 (2015).
5. G. Talli, S. Porto, D. Carey, N. Brandonisio, A. Naughton, P. Ossieur, F. Slyne, S. McGettrick, C. Blum, M. Ruffini, D. Payne, R. Bonk, T. Pfeiffer, N. Parsons, and P. Townsend, "Demonstration of SDN Enabled Dynamically Reconfigurable High Capacity Optical Access for Converged Services," in *Optical Fiber Communication Conference* (OFC) Postdeadline Papers, OSA Technical Digest (online) (Optical Society of America, 2016), paper Th5B.1.
6. G. Talli, F. Slyne, S. Porto, D. Carey, N. Brandonisio, A. Naughton, P. Ossieur, S. McGettrick, C. Blumm, M. Ruffini, D. Payne, R. Bonk, T. Pfeiffer, N. Parsons, and P. Townsend, "SDN Enabled Dynamically Reconfigurable High Capacity Optical Access Architecture for Converged Services," J. Lightwave Technol. **35**(3), 550–560 (2016).
7. D. Carey, N. Brandonisio, S. Porto, A. Naughton, P. Ossieur, N. Parsons, G. Talli, and P. Townsend, "Dynamically Reconfigurable TDM-DWDM PON Ring Architecture for Efficient Rural Deployment," in *European Conference on Optical Communication* (ECOC, 2016).

8. R. P. Davey, D. B. Grossman, M. Rasztovits-Wiech, D. B. Payne, D. Nesset, A. E. Kelly, A. Rafel, S. Appathurai, and S. H. Yang, "Long-Reach Passive Optical Networks," J. Lightwave Technol. **27**(3), 273–291 (2009).
9. R. Bonk, H. Schmuck, W. Poehlmann, and T. Pfeiffer, "Long Reach Passive Optical Network Architectures," Photonic Networks; 15. ITG Symposium (2014), pp. 1–5.
10. M. Ruffini, L. Wosinska, M. Achouche, J. Chen, N. Doran, F. Farjady, J. Montalvo, P. Ossieur, B. O'Sullivan, N. Parsons, T. Pfeiffer, X. Qiu, C. Raack, H. Rohde, M. Schiano, P. Townsend, R. Wessaly, X. Yin, and D. B. Payne, "DISCUS: an end-to-end solution for ubiquitous broadband optical access," IEEE Commun. Mag. **52**(2), S24–S32 (2014).
11. V. Houtsma, D. V. Veen, and E. Harstead, "Recent Progress on 25G EPON and beyond," in *European Conference on Optical Communication* (ECOC, 2016).
12. D. T. van Veen and V. E. Houtsma, "Symmetrical 25-Gb/s TDM-PON With 31.5-dB Optical Power Budget Using Only Off-the-Shelf 10-Gb/s Optical Components," J. Lightwave Technol. **34**(7), 1636–1642 (2016).
13. H. S. Abbas and M. A. Gregory, "The next generation of passive optical networks: A review," J. Netw. Comput. Appl. **67**, 53–74 (2016).
14. A. Shahpari, R. M. Ferreira, R. S. Luis, Z. Vujicic, F. P. Guiomar, J. D. Reis, and A. L. Teixeira, "Coherent Access: A Review," J. Lightwave Technol. **35**(4), 1050–1058 (2017).
15. S. J. Savory, "Digital coherent optical access networks," in *IEEE Photonics Conference* (2013).
16. D. Lavery, R. Maher, D. S. Millar, B. C. Thomsen, P. Bayvel, and S. J. Savory, "Digital Coherent Receivers for Long-Reach Optical Access Networks," J. Lightwave Technol. **31**(4), 609–620 (2013).
17. N. Suzuki, S. Yoshima, H. Miura, and K. Motoshima, "Demonstration of 100-Gb/s/λ-Based Coherent WDM-PON System Using New AGC EDFA Based Upstream Preamplifier and Optically Superimposed AMCC Function," J. Lightwave Technol. **35**(8), 1415–1421 (2017).
18. I. N. Cano, J. Prat, J. Tabares, J. C. Velasquez, S. Ghasemi, V. Polo, G. Y. Chu, M. Presi, E. Ciaramella, M. Rannello, F. Bottoni, M. Artiglia, G. Cossu, R. Pous, G. Azcarate, C. Vila, H. Debregeas, G. Vall-llosera, and A. Rafel, "Field-Trial of Low-Cost Coherent UDWDM-PON with Real-Time Processing, λ-Monitoring and EPON Coexistence," in *42nd European Conference on Optical Communication* (ECOC, 2016).
19. A. Teixeira, A. Shahpari, R. Ferreira, F. P. Guiomar, and J. D. Reis, "Coherent access," in *Optical Fiber Communications Conference and Exhibition* (OFC, 2016).
20. R. Koma, M. Fujiwara, J. Kani, S.-Y. Kim, T. Suzuki, K.-I. Suzuki, and A. Otaka, "Demonstration of Real-Time Burst-Mode Digital Coherent Reception With Wide Dynamic Range in DSP-Based PON Upstream," J. Lightwave Technol. **35**(8), 1392–1398 (2017).
21. A. Bononi, M. Bertolini, P. Serena, and G. Bellotti, "Cross-Phase Modulation Induced by OOK Channels on Higher-Rate DQPSK and Coherent QPSK Channels," J. Lightwave Technol. **27**(18), 3974–3983 (2009).
22. H. Griesser and J. P. Elbers, "Influence of cross-phase modulation induced nonlinear phase noise on DQPSK signals from neighbouring OOK channels," in *European Conference on Optical Communication* (ECOC, 2005).
23. O. Bertran-Pardo, J. Renaudier, G. Charlet, H. Mardoyan, P. Tran, and S. Bigo, "Nonlinearity Limitations When Mixing 40-Gb/s Coherent PDM-QPSK Channels With Preexisting 10-Gb/s NRZ Channels," IEEE Photonics Technol. Lett. **20**(15), 1314–1316 (2008).
24. S. Chandrasekhar and X. Liu, "Impact of Channel Plan and Dispersion Map on Hybrid DWDM Transmission of 42.7-Gb/s DQPSK and 10.7-Gb/s OOK on 50-GHz Grid," IEEE Photonics Technol. Lett. **19**(22), 1801–1803 (2007).
25. H. Griesser, J. P. Elbers, H. Wernz, and C. Fürst, "43 Gb/s RZ-DQPSK Transmission over a 660 km 10.7 Gb/s DWDM Link," in *European Conference on Optical Communications* (ECOC, 2006).
26. D. Lavery, M. Ionescu, S. Makovejs, E. Torrengo, and S. J. Savory, "A long-reach ultra-dense 10 Gbit/s WDM-PON using a digital coherent receiver," Opt. Express **18**(25), 25855–25860 (2010).
27. A. Kaszubowska-Anandarajah, R. Oberland, E. Bravi, A. Surpin, O. Aharoni, U. Ghera, R. Giller, E. Connolly, E. K. MacHale, M. Todd, G. Talli, and D. McDonald, "EDFA transient suppression in optical burst switching systems," 14th *International Conference on Transparent Optical Networks* (ICTON, 2012).
28. ITU-T recommendation G.671.
29. S. J. Savory, "Digital filters for coherent optical receivers," Opt. Express **16**(2), 804–817 (2008).
30. J. Viterbi and A. M. Viterbi, "Nonlinear Estimation of Psk-Modulated Carrier Phase with Application to Burst Digital Transmissions," IEEE Trans. Inf. Theory **29**(4), 543–551 (1983).
31. J. G. Proakis, *Digital Communications*, 4th Ed. (McGraw-Hill, 2001).
32. M. K. Simon and M. S. Alouini, *Digital Communication over Fading Channels – A Unified Approach to Performance Analysis*, 1st Ed. (Wiley, 2000).
33. D. d. Borne, C. R. S. Fludger, T. Duthel, T. Wuth, E. D. Schmidt, C. Schulien, E. Gottwald, G. D. Khoe, and H. de Waardt, "Carrier phase estimation for coherent equalization of 43-Gb/s POLMUXNRZ- DQPSK transmission with 10.7-Gb/s NRZ neighbours," in *European Conference and Exhibition of Optical Communication* (2007).
34. G. Agrawal, *Applications of Nonlinear Fiber Optics* (Academic Press, 2010).

1. Introduction

The development of future access networks will be driven by the need to enable increasing traffic volumes while delivering heterogeneous service types that may require different

modulation formats on a single common physical layer [1-3]. A key challenge therefore, is how to support the convergence of a wide set of services that will likely need to be offered in a dynamically reconfigurable and ubiquitous manner - 'anytime', 'anywhere' - over a single shared network infrastructure. Within the access network, passive optical networks (PONs) are particularly suited to reach a large number of customer end-points with a transparent infrastructure and a single fiber connection to the local exchanges. By taking advantage of the dynamic allocation of dense wavelength division multiplexing (DWDM) channels over the PONs, the demands of multiple service and optical channel types can also be satisfied. For example, the same access infrastructure could use different wavelength channels to deliver parallel heterogeneous services based on different modulation formats such as shared 10Gb/s PON services to residential customers, dedicated point-to-point (P2P) 100Gb/s services to business customers, and wireless fronthaul [4-7]. These channel allocations can then evolve over time in response to changing demand. An overall network de-layering and consolidation can also be achieved by combining the concepts of a long-reach PON (LR-PON [8, 9]) in the access and a flat optical core arranged into islands of transparency [10]. This approach exploits the physical reach of LR-PONs to enable the concentration of many PON fiber terminations into a smaller number of nodes, each covering large areas, thus enabling the consolidation of a substantial number of electronic packet switching nodes [10], reducing capital and operating costs. While current PON standards support single channel line rates of up to 10Gb/s [1], the effort of the standardization activities is focused at the moment on increasing the single channel rate to 25Gb/s, which employing four wavelengths will enable an overall capacity of 100Gb/s per PON [11-13]. Despite being further into the future of the standardization roadmap, higher bit-rates of up to 100Gb/s per channel were also demonstrated by using coherent technologies [14-17] in a PON system. The coexistence of these new services with legacy PON systems has also been discussed [4, 18-20].

The present investigation builds upon these concepts and addresses the feasibility of the proposed coexistence in LR-PON systems of a high capacity P2P 100Gb/s channel for business services and high dynamic range, burst-mode traffic of 10Gb/s on-off keying (OOK) time division multiplexed (TDM) shared channels for residential type services. Dual-polarization quadrature phase-shift keying (DP-QPSK) was chosen in this work as the modulation format for the 100Gb/s dedicated P2P link since it is the most commonly adopted solution by the telecommunication industry for 100Gb/s long haul and metro optical channels. In the absence of active power leveling, LR-PONs can exhibit high burst-to-burst dynamic range in the upstream channels due to a large differential loss in the optical distribution network (ODN). Hence, a DP-QPSK 100Gb/s P2P channel may be impaired by nonlinear crosstalk from high power neighboring 10Gb/s OOK PON channels. Whilst 100G/10G channel coexistence has been widely studied in the context of metro and long-haul networks, this is the first time to our knowledge that such an in-depth study has been carried out in the context of PONs, where the unique additional constraint of burst mode traffic support is a critical factor.

The potential for coexistence is investigated here for two LR-PON architectures, the first one particularly suited for densely populated areas, and a second one aimed at rural, sparsely populated areas. Figure 1(a) shows a high-level view of a tree LR-PON architecture suited for densely populated areas [5-6], which incorporates a TDM-DWDM LR-PON and a flat optical core. As the amplifier nodes (ANs) in this design serve hundreds of residential and potentially business users, they are dual parented for protection with a secondary backhaul link to a geographically separated core node (CN). In sparsely populated rural areas, on the other hand, the communities to be served can be much smaller than the total LR-PON split of conventional tree structures. This would result in a considerably underutilized network infrastructure with a consequent increased cost per customer. An alternative structure based on a chain of amplifier nodes (ANs) has recently been proposed to improve the utilization and efficiency of fiber-based access for rural, sparsely populated areas [7]. Figure 1(b) presents a

high-level design view of this novel LR-PON configuration. This architecture is based on the structure of metro rings, where two fibers with counter-propagating traffic connect a chain of nodes and it has the added advantage of directly reusing the ring fiber topologies deployed in today's metro networks. The ring is open and the two head-ends are two CNs, while the intermediate nodes are the AN sites where the ODNs are optically aggregated into the LR-PON. Similar to the tree structure, the chain of ANs (also called open-ring architecture in the remainder of this paper) is dual parented for protection on two geographically separated CNs of a flat optical core network. This architecture presents the same intrinsic resilience as metro rings, where if there is a failure in the active CN, in an AN node, or there is a fiber cut, the traffic can be routed to and from the protection CN.
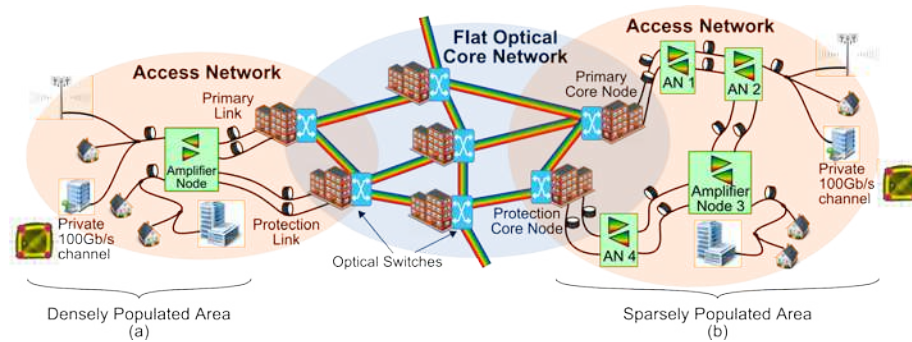

Fig. 1. High-level network view of: (a) a conventional tree LR-PON architecture for densely populated areas; (b) a novel LR-PON architecture based on a chain of amplifier nodes for rural deployment.

The influence of cross-phase modulation (XPM) on DP-QPSK signals from neighboring OOK channels is a key issue for hybrid coherent optical systems and it has been extensively discussed in the context of long-haul and metro networks in recent years [21–26]. However, to the best of our knowledge, this is the first time that a detailed analysis has been carried out specifically in the context of a LR-PON system taking into account realistic power variations associated with the burst-mode nature of the upstream link and supporting a physical reach of at least 100km, 512 users and an emulated traffic load of 40 channels. In contrast to long-haul and metro systems, where the channels are characterized by the same launched average optical power (i.e. zero dynamic range), this paper presents a number of unique case studies where large dynamic ranges between the PON channels are taken into account in the upstream direction for both network architectures mentioned above. Furthermore, while the downstream link of long-haul and metro systems is typically optical signal-to-noise ratio (OSNR)-limited as a consequence of the fairly homogeneous amplifier spacing and topologies, in this work downstream links with non-uniform amplifier distributions are also taken into account. This represents a unique case of study where the link is characterized by OSNR- as well as power-limited operation due to the large lumped losses in the ODN section. It should be noted that the non-uniform amplifiers distribution, along with the large lumped losses in the ODN, have also a direct impact on the minimum required launched power into the various fiber spans. As a consequence, fiber nonlinearities may have different effects on the upstream and downstream channels of the two network topologies due to the asymmetric nature of their links.

The work described in this paper begins by presenting both test-beds corresponding to the network architectures illustrated in Figs. 1(a) and 1(b), which are described in detail in Section 2. The corresponding experimental results are then discussed in Section 3. Section 4 describes the experimental results obtained from the characterization of the 100G transponder in back-to-back (B2B) as well as in a simplified transmission setup (80km of fiber, with only two 10Gb/s OOK neighboring channels) that allowed the impact of nonlinearities to be

evaluated. These results have been used to construct and validate a numerical model that can be employed to optimize the system performance and to extract useful information not otherwise obtainable in a lab environment. Finally, Section 5 presents a comprehensive study using the system model to optimize the design of both network architectures proposed for urban and rural areas and to evaluate the performance of the 100G channel for alternative node distributions and locations in the AN chain case.
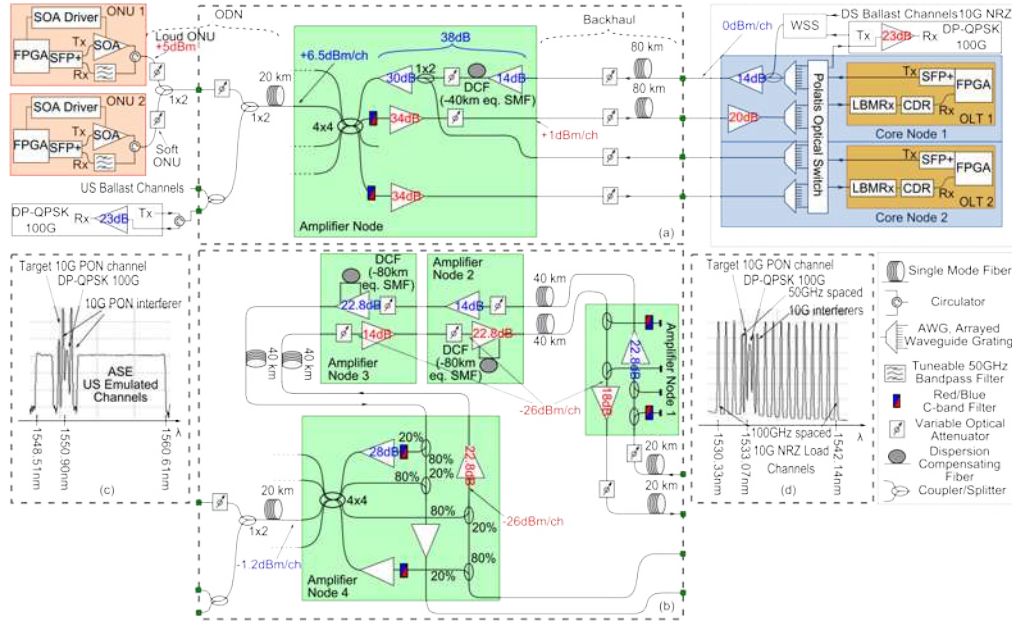

Fig. 2. Physical layer experimental setup of the LR-PON architecture for (a) urban densely populated areas, and (b) rural sparsely populated areas; (c) upstream and (d) downstream spectra.

2. Test-bed description

Figure 2 presents the details of the experimental physical layer for both LR-PON architectures. The conventional tree topology for urban, densely populated areas is illustrated in Fig. 2(a), while a novel LR-PON design based on a chain of ANs for rural, sparsely populated areas is illustrated in Fig. 2(b). In the CN, a DWDM multiplexer and an optical space switch (Polatis model N-VST-24×24-LU1-MMHNS-300) are used to route the upstream and downstream of either PON or P2P channel to the relative optical line terminal (OLT) receiver (Rx) and transmitter (Tx) respectively, providing the capability to re-configure the wavelength allocations [6]. A second CN is connected to the AN (AN 4 for the rural deployment case) to provide resilience and protection. The same optical network units (ONUs) and CNs are connected to both LR-PON test-beds by means of a second optical space switch (Polatis model I-VST-32×32-FA1-GSENS-200) used for experimental convenience to reliably interchange between the two network designs. Figure 2 also shows the details of the ODNs, of the backhaul links and the details of the AN designs, such as amplifier gains and channel powers. It should be noted that in both architectures, all of the erbium-doped fiber amplifiers (EDFAs) used for upstream transmission are commercial devices with fast gain stabilization in order to reduce the impact of gain transients induced by the burst traffic [27]. Attenuators are added in the ODNs to emulate the end-of-life standard single mode fiber (SMF) attenuation (0.3dB/km) and realistic splitter losses including excess loss [28]. Throughout this work we consider a worst case loss of 3.5dB for each × 2 split in the ODN loss calculations. For both architectures the span of the ODN is 20km and part of

the total ODN split (4 × 4) is located in the AN, which is also used to separate and combine the upstream and downstream channels and to provide access to the redundancy path used for protection. The lengths of the fiber links for the two architectures are indicated in Fig. 2. In the open-ring system presented in Fig. 2(b), ANs 1 and 4 are fully implemented while ANs 2 and 3 are only partially implemented with no fiber in between the two nodes in order to emulate AN co-location which facilitates the provision of a larger split in a specific area. The total reach of the LR-PON for the tree architecture is 100km, while the open-ring setup is 120km in length.

The 100G P2P channel is realized using a commercial transponder to generate and receive the DP-QPSK signal. It should be noted that the transponder includes an internal soft-decision forward error correction (SD-FEC) encoding technology that uses a low density parity check (LDPC) code. The associated overhead pushes the actual line rate up to 128Gb/s. Throughout this work, however, only the pre-FEC bit error rate (BER) is measured, which is obtained from the FEC decoder, and for simplicity an FEC threshold of 1.1E-3 was assumed, as in the case of the 10Gb/s PON channels [6]. The optical carrier wavelength for the DP-QPSK channel was set to 1533.47nm and 1551.32nm for the downstream and upstream channels respectively. Two OLTs and two ONUs are fully implemented, and additional traffic equivalent to a power of 40 channels in both upstream and downstream is added to fully load the network. Figure 2(c) shows the upstream band, where the additional channels are emulated using amplified spontaneous emission (ASE), which is filtered and flattened using a wavelength selective switch (WSS). The power of both 50GHz-spaced OOK channels adjacent to the DP-QPSK channel is swept to emulate optical bursts experiencing different ODN losses, while the power of a third OOK channel located at 100GHz from the DP-QPSK channel is maintained at the nominal power level (i.e. in the middle of the PON channel dynamic range). The ASE power is set in order to obtain an overall upstream power equivalent to 40 channels at nominal power. In the downstream transmission band, the additional channels are emulated using 15 DFB lasers externally modulated at 10Gb/s with non-return to zero (NRZ) OOK pseudorandom data using a LiNbO3 Mach-Zehnder modulator. The corresponding power spectra are shown in Fig. 2(d). The power of these additional channels is set equal to nominal power for the four channels neighboring the 100G channel (two at lower wavelengths and two at higher wavelengths), while the power of the remaining 13 channels is adjusted in order to obtain an overall downstream power equivalent to 40 channels at nominal power. For experimental convenience the additional downstream channels, coupled into the system at the CN, after the Polatis optical switch and before the booster amplifier, are always present, which allows the use of simpler EDFA controls in the downstream link.

3. Experimental results

In this section the experimental results obtained from the physical layer characterization of the 100G DP-QPSK private channel are discussed for both network architectures presented in the previous sections. It should be noted that the analysis of the 10Gb/s PON channels is not reported here as the focus of this paper is on the 100G performance only. However, the reader can refer to [5–7] for a detailed description of the 10Gb/s PON channel experimental results.

3.1 Downstream

In the downstream direction, the 100G link was characterized as a function of the ODN loss, as shown in Fig. 3(a). The 100G channel performance is impaired by OSNR degradation as well as by the nonlinear fiber effects. Due to limitations introduced in the set-up by the insertion loss of the WSS, the optical coupler, and the various passive elements in between, the maximum OSNR of the DP-QPSK signal at the output of the CN was 26dB. While this is highly unlikely to occur in a real network, where the transmitted OSNR should be significantly higher, it represents a worst case scenario study. For high ODN loss the OSNR

is limited by the ASE introduced by the pre-amplifier EDFA. The difference of approximately 8dB at FEC threshold between the experimental curves relative to the two network designs corresponds closely to the difference in the 100G signal powers launched into the ODN (i.e. + 6.5dBm for tree architecture against −1.2dBm for the open-ring). On the other hand, for a low ODN loss the maximum achievable OSNR is limited by the AN and CN amplifiers and it is equal to ~23dB and ~21dB for the tree and the open-ring designs respectively. From the experimental curves in Fig. 3(a) it is possible to see that for low ODN loss, despite the higher OSNR, the tree architecture has poorer performance than the open-ring architecture due to the higher impact of the nonlinear crosstalk with the 10Gb/s OOK channels in the fiber. This results in a BER floor approximately one order of magnitude higher than the open-ring design (~1E–4 versus ~1E–5).
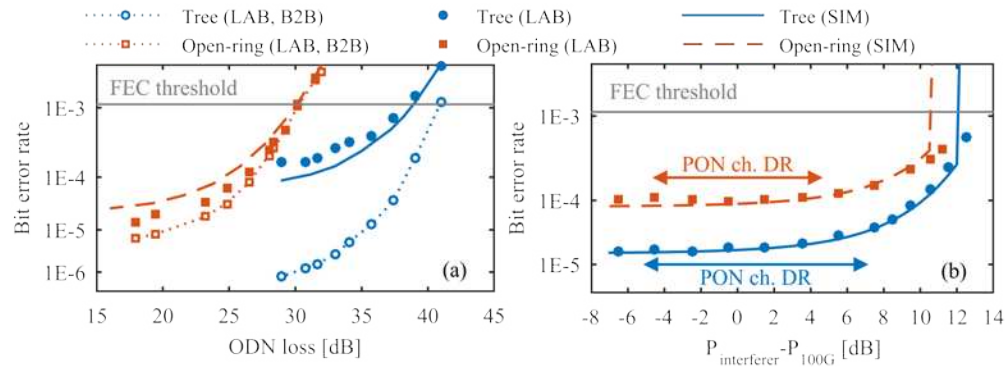

Fig. 3. Experimental results vs. modeling: (a) performance of the 100G link in downstream as a function of the ODN loss; (b) performance of the 100G link in upstream as a function of the power of the neighboring OOK PON channels.

In order to evaluate the effect of nonlinearities for both network schemes in more detail, Fig. 3(a) also shows the BER measured as a function of the ODN loss in B2B, where the output of the CN is connected directly to the pre-amplifier EDFA and all of the 10Gb/s OOK channels have been disabled. In this case the ODN loss is emulated by a variable optical attenuator (VOA) which changes the OSNR at the input of the coherent receiver. Assuming a negligible impact from other sources of impairments, such as chromatic dispersion, the effect of the nonlinearities can be clearly seen by comparing the B2B curves for both network designs with the corresponding curves obtained with the respective LR-PON. In the tree architecture, the effect of nonlinearities is highly visible, as the BER floor increases by approximately two orders of magnitude in comparison to the B2B case. On the other hand, in the open-ring architecture the effect of nonlinearities is rather small as shown by the experimental curve in Fig. 3(a) which almost lies on the top of the B2B measurements. This is due to the fact that in the open-ring design the maximum power launched into the various fiber links (≤0dBm) is significantly smaller than in the tree design (≤6.5dBm) because of the more closely spaced amplifiers and more distributed losses. Therefore, despite the fact that in the open-ring case there is an accumulated effect of XPM from the multiple fiber links, this is still negligible in comparison to the effect of XPM from the backhaul link of the tree architecture.

Assuming an FEC threshold of 1.1E-3, the experimental curves of Fig. 3(a) show that the conventional tree structure can support a 100G link with an ODN loss of up to ~38.5dB, which corresponds to 128 split with 20km of distribution fiber and ~8dB of system margin. Considering the additional split in the AN, the overall split ratio supported by the tree design is 128 × 4 = 512, which could be further increased at the expense of the ~8dB system margin. Similarly, the open-ring architecture can support the 100G channel with ODN loss up to ~30dB, which corresponds to 64 split with 20km of distribution fiber and ~3dB system

margin. Or in total, 64 × 4 = 256 splits when the additional split in AN 4 is taken into account, and 256 × 4 = 1024 users when all intermediate ANs are aggregated.

3.2 Upstream

In the upstream direction the OOK PON traffic, which interferes with the 100G channel, comprises bursts of different powers. In the conventional tree architecture, the non-uniform ODN loss can cause up to 12dB of dynamic range between burst powers, while in the open-ring design the resulting dynamic range can be up to 9dB under the assumption that, for simplicity, all ONUs (OOK and 100G) have the same launch power of + 5dBm. These values have been estimated considering a 512 and a 256 split ratio for the two network architectures respectively, and realistic splitter losses [28]. The experimental values of the nominal ODN loss (28.6dB and 24dB respectively for the tree-design and the open ring design) are slightly higher than the ODN loss that would be obtained considering a worst case loss of 3.5dB for each × 2 split, which represents a worst case in terms of achieved OSNR for the DP-QPSK signal as well as for the 10Gb/s PON channels. The 100G channel was characterized in terms of penalty caused by the nonlinear crosstalk from the two neighboring 10Gb/s OOK PON channels bursting with high power, as this represents a realistic worst case. The BER of the 100G upstream link was measured as a function of the power of two 50GHz-spaced interfering channels operated with 2μs bursts and 2μs gaps overlapped in time to also provide a worst case for the nonlinearity.

The experimental results in Fig. 3(b) show that for small OOK channel powers the BER of the tree architecture is almost an order of magnitude lower than the open-ring architecture, due to the fact that in the first case it is possible to achieve a ~2dB higher OSNR (~21.5dB versus ~19.5dB). In contrast to the downstream case, the maximum launched power into the various fiber links is very similar for both network architectures. This corresponds to approximately −4dBm into the 80km backhaul fiber for the tree design, as well as into the two 40km links for the open-ring design. As a consequence, the performance of both architectures degrades with a similar trend and for high power of the OOK channels the experimental curves tend to converge towards the FEC threshold for OOK channel powers ~12dB higher than the DP-QPSK channel power. Figure 3(b) also indicates the dynamic ranges expected from a non-uniform ODN loss for tree design (12dB) and for the open-ring design (9dB). The 100G channel can work below FEC threshold even when the neighboring bursty channels present dynamic ranges larger than the values induced by the non-uniform ODN loss. It should also be noted that, while in the open-ring case the dynamic range is distributed symmetrically around the nominal value, in the tree design the dynamic range is asymmetric with −5dB and + 7dB. This is caused in the experiment by misalignment of 1dB between the ODN loss range and the LBMRx dynamic range. In the modeling results presented in the Section 5 this issue has been corrected with a symmetric dynamic range around the nominal value. This also demonstrates the importance of an accurate model in order to optimize the system design.

4. Modeling results

One of the main objectives of this work is to develop a system model that can be used to optimize the design of both network architectures discussed above and the first step is to develop an accurate model for the 100G transponder. The 100G transponder was first experimentally characterized in B2B by connecting the output of the CN directly to the pre-amplifier EDFA with all the 10Gb/s OOK channels off and bypassing the LR-PON. The 100G signal was filtered using a WSS (50GHz ITU grid) and the pre-FEC BER measured as a function of the OSNR, as shown in Fig. 4(a). The OSNR was set by varying the optical power at the input of the pre-amplified receiver. Next, the performance of the transponder was evaluated in terms of nonlinear impairments such as self-phase modulation (SPM) and cross-phase modulation (XPM) from two 10Gb/s OOK neighboring channels (one at a lower and

one at a higher wavelength respectively). In order to do so, the signal from the CN was sent over the 80km backhaul link and then directly to the pre-amplified receiver bypassing the AN and the ODN. The performance of the transponder in terms of SPM was evaluated by measuring the BER as a function of the 100G signal power launched into the fiber for different OSNRs, as shown in Fig. 4(b). Note that in this case the two OOK neighboring channels were disabled. Finally, the performance in terms of XPM was evaluated by enabling two OOK channels, first at ± 50GHz and then at ± 100GHz from the DP-QPSK target signal, under the assumption that most of the penalty is caused by the two neighboring channels. For this preliminary study the two OOK channels were operated in continuous-mode, as this represent the worst case scenario (continuous effect of crosstalk). The BER was measured as a function of the OOK channel power launched into the fiber and for a constant DP-QPSK signal power of + 10dBm. The relative curves are shown in Figs. 4(c) and 4(d) for the 50GHz and 100GHz channel spacing cases respectively.
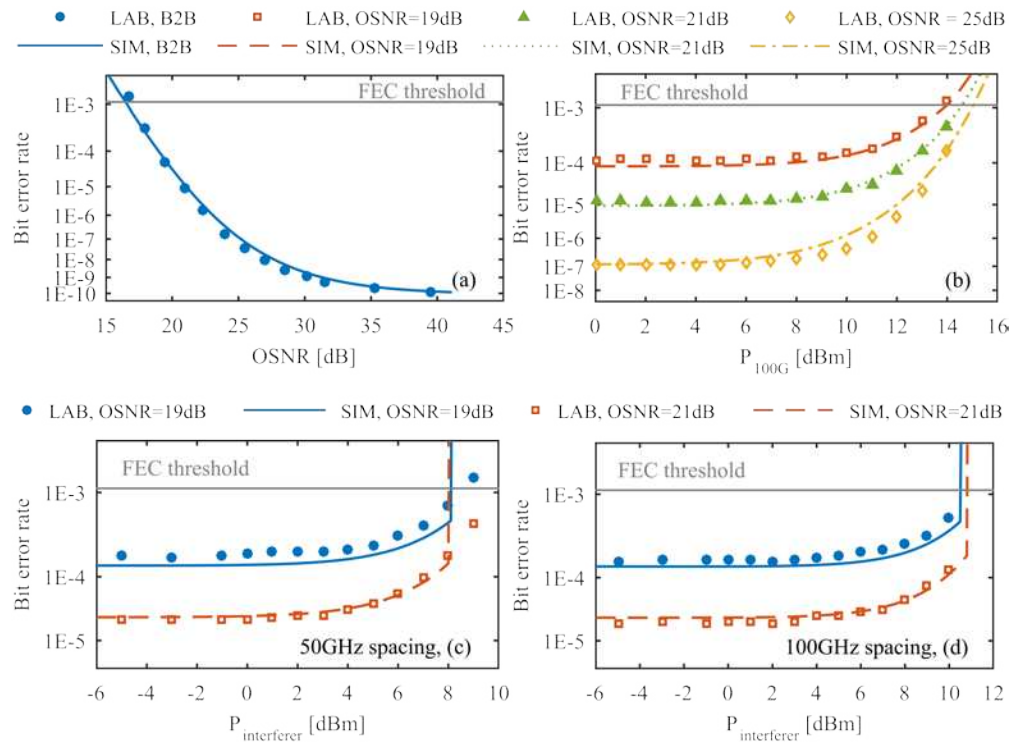

Fig. 4. Experimental results vs. modeling: (a) B2B performance; (b) impact of SPM on the DP-QPSK channel performance; impact of XPM on the DP-QPSK channel performance for (c) 50GHz- and (d) 100GHz-spaced 10Gb/s OOK neighboring channels.

Using VPItransmissionMaker, a model for the 100G transponder was developed in order to reproduce the characterization results presented in Fig. 4. Each polarization was I/Q modulated using 32Gb/s NRZ, de-correlated, 2^7-1 pseudo random bit sequence (PRBS) data. The simulated coherent receiver block included digital signal processing (DSP) and symbol error rate (SER) estimation based on Gaussian methods (for simplicity, only the results relative to the X-polarization were monitored). The DSP section incorporates digital filtering for chromatic dispersion (CD) compensation (60 taps when the signal inside the DSP block is resampled at twice the symbol rate [29]) and an adaptive, blind, multiple-input multiple-output (MIMO) equalizer based on the constant modulus algorithm (CMA) (7 taps, 30 iterations, step-size 0.005) for polarization dependent impairment compensation, as well as a carrier phase estimation (CPE) block employing the Viterbi & Viterbi algorithm [30] using 17

symbols averaging. The two 10Gb/s OOK channels used to stress the DP-QPSK signal were also modulated using 2^7-1 PRBS data. A summary of the main system parameters that allowed an accurate fit of the experimental curves is reported in Table 1. Since the commercial transponder performance was evaluated in terms of BER while the model provided SER estimation, the latter was converted to BER by solving the following system of error probability equations for a QPSK signal [31, 32]:

$$SER = 2Q\left(\sqrt{\frac{2E_b}{N_0}}\right)\left[1 - \frac{1}{2}Q\left(\sqrt{\frac{2E_b}{N_0}}\right)\right], \qquad (1)$$

$$BER = Q\left(\sqrt{\frac{2E_b}{N_0}}\right), \qquad (2)$$

where $Q(\cdot)$ is the Q-function, E_b is the energy per bit and N_0 is the noise power spectral density. In the case of large symbol signal-to-noise ratio, Eq. (1) and Eq. (2) lead to BER $\approx$SER/2.

Table 1. Summary of Main Simulation Parameters

Tx/Rx electrical bandwidth	9 GHz (order 1)	PMD coefficient	0.1E-12/31.62
Rx-WSS optical bandwidth	50 GHz (order 4)	Fiber group refractive index	1.47
Tx-laser linewidth	0.1 MHz	Fiber nonlinear index	2.6E-20 m²/W
Local oscillator linewidth	0.1 MHz	Fiber core area	80.0E-12 m²
Down-/Up-stream wavelength	1533.47/1551.32nm	DSP sampling rate	64 GSa/s
OOK extinction ratio	10 dB	n. taps (CD equalizer)	60
EDFAs noise figure	5.5dB	n. taps (MIMO equalizer)	7
Fiber attenuation	0.2 dB/km	Step-size for CMA	0.005
Fiber dispersion	16E-6 s/m²	n. of iterations for CMA	30
Fiber dispersion slope	0.057E3 s/m^3	n. of symbols used for CPE	17

From Fig. 4(a) it is possible to see that the transponder model is able to precisely reproduce the B2B data, with a good match at small OSNRs around the FEC threshold as well as at high OSNRs, where the BER floors at a value of ~1E-10. With regard to the SPM analysis, Fig. 4(b) also shows a good match between experimental data and modeling results for all OSNR cases taken into account. It is possible to note that SPM starts to have an impact on performance only for launched powers greater than approximately + 10dBm, after which the BER curves increase rapidly. On the other hand, the effect of XPM on the DP-QPSK channel becomes noticeable at much lower powers, i.e. approximately + 5dBm and + 8dBm for 50GHz- and 100GHz-spaced channels respectively, as shown in Figs. 4(c) and 4(d). Once again, the model is able to provide a good match to the experimental results up to OOK powers where the DSP block is no longer effective in reconstructing the transmitted data from the received signal. As a consequence, for these OOK powers the simulated BER increases dramatically exceeding the FEC limit. This behavior is attributed to the XPM-induced phase noise that impairs the CPE process [33]. Averaging over a shorter interval for CPE is known to reduce but not eliminate this issue, as the XPM-induced phase changes cannot be completely averaged out. Hence, more tolerant CPE schemes or nonlinear compensation schemes should be employed to obtain a significant improvement.

The model has been used to study the two network architectures and to reproduce the experimental data previously presented in Fig. 3. The performance of the 100G DP-QPSK channel (128Gb/s in total to allow for forward error correction (FEC) overhead, as for the experimental setup) for the two network architectures has also been modeled using VPItransmissionMaker. In the downstream case, ten neighboring OOK channels adjacent to the DP-QPSK channel were included. Using as reference Fig. 2(d), this corresponds to the five channels at either side of the 100G channel, including a 50GHz spaced channel at either

side. In order to simplify the simulation test-bed, in the upstream case the ASE used to emulate the additional PON channels was not modeled. Only the three OOK channels adjacent to the DP-QPSK channel were included, as shown in Fig. 2(c), as most of the penalty on the 100G channel is due to the nonlinear crosstalk from the adjacent channels. As for the experimental case, the optical carrier for the DP-QPSK transmitter was set to 1533.47nm and 1551.32nm for the downstream and upstream respectively (100kHz linewidth assumed for both transmitter and receiver). Figure 2 can also be used as a reference for the details on the simulation setup, such as power levels, amplifier gains, etc. All the EDFAs used in the simulations had a noise figure of 5.5dB. It should be also noted that in the simulation setup the fiber loss was set to 0.2dB/km and the remaining 0.1dB/km was added as additional attenuation after the fiber in order to account for an end-of-life loss of 0.3dB/km. This represents the worst case scenario in terms of nonlinearities.

The results obtained in the downstream case from the tree and open-ring architecture full system models are shown in Fig. 3(a). From these curves it is possible to see that the model is in good agreement with the experimental data, with an accurate fit around FEC threshold and only a negligible discrepancy in the BER floor value for both network architectures. This confirms that the tree design can support $128 \times 4 = 512$ splits with ~8dB system margin, while the open-ring architecture $64 \times 4 = 256$ splits per AN (i.e. $256 \times 4 = 1024$ users when all ANs are aggregated) with ~3dB system margin. With regard to the upstream case, from Fig. 3(b) it is possible to see that the model is in good agreement with the experimental results up to the point where the XPM-induced phase noise impairs the CPE process, as discussed above. However, this only happens for relatively high OOK channel powers that would correspond to unrealistic dynamic ranges. It should be noted that in the upstream direction only continuous-mode (CM) operation was emulated with VPI, which would corresponds to a case where the interfering bursts are always transmitting at the maximum power. Hence, in order to scale the continuous mode modeling results to the same burst-mode (BM) conditions of the experiments, the following equation was applied:

$$BER_{BM}\left(P_{OOK}\right) = \frac{1}{2}BER_{CM}\left(P_{OOK}\right) + \frac{1}{2}BER_{CM,0}, \qquad (3)$$

where P_{OOK} is the power of the OOK channels at which the BER is measured, P_{100G} is the nominal power of the DP-QPSK signal and $BER_{CM,0}$ represents the BER of the 100G channel when there is no effect from the OOK channels $\left(P_{OOK} \ll P_{100G}\right)$. Equation (3) is valid when the bursts present a duty-cycle of 50% and under the assumption that the nonlinear response of silica fibers is almost instantaneous (<10fs [34]) and thus negligible compared to the burst period of a few microseconds.

5. Network design optimization

The excellent agreement between measurements and modeling results for all the cases presented in Sections 3 and 4 is a validation of the modeling approach used here. This means that the model can also be used to predict the system performance and to carry out a network optimization when some of the main design parameters such as launched powers, amplifiers gain, fiber length, etc., are changed. In fact, the specific implementations of both network architectures discussed in the previous sections were imposed by the availability of lab components at that time, and does not necessary represent the optimum solution in terms of cost and performance. The modeling results presented in this section can therefore be used as a valuable means to optimize those design parameters and to provide insights that might be harder to obtain from a more complicated and less controllable real-world environment. Figures 5(a) and 5(b) illustrates a simplified high-level overview of the two simulation setups employed to model the tree and open-ring LR-PON architectures.

Alternative architecture topologies can also be studied by using the model. While the conventional tree design is typically characterized by a long backhaul fiber (≤100km) and a unique AN that serves all the customers in an urban area within a radius of ≤20km, the open-ring architecture presents a much more flexible design that is better able to adapt to sparsely populated communities in different and non-uniform geographically separated areas. This architecture is based on a chain of ANs whose distance from each other can adapt to the territory morphology and to the location of powered street cabinets or local exchanges that will house the ANs. The distance between consecutive ANs can also adapt based on the actual location as well as the size of the various communities, for example by co-locating two distinct ANs as shown in the previous sections. Therefore the fiber configuration for the open-ring architecture presented in the previous sections represents only one of many possible cases of study. The parameter space of the open ring topologies is very large, but in order to demonstrate the high flexibility of this novel open-ring design, two more cases have been identified as the extremes in terms of fiber length and nonlinearities. The first case taken into account emulates an equal distribution of fiber spans between the ANs with a distance of 25km from each other (as well as from the CN to AN 1), as illustrated in Fig. 5(c). This open-ring design is representative of a worst-case scenario in terms of accumulation of nonlinearities over the multiple fiber links. The second open-ring design, instead, is representative of a worst-case scenario in terms of maximum span distance and hence in terms of the maximum power launched into the fiber. In this case the fiber links are unequally distributed with only 2 × 50km fiber spans, as illustrated in Fig. 5(d).
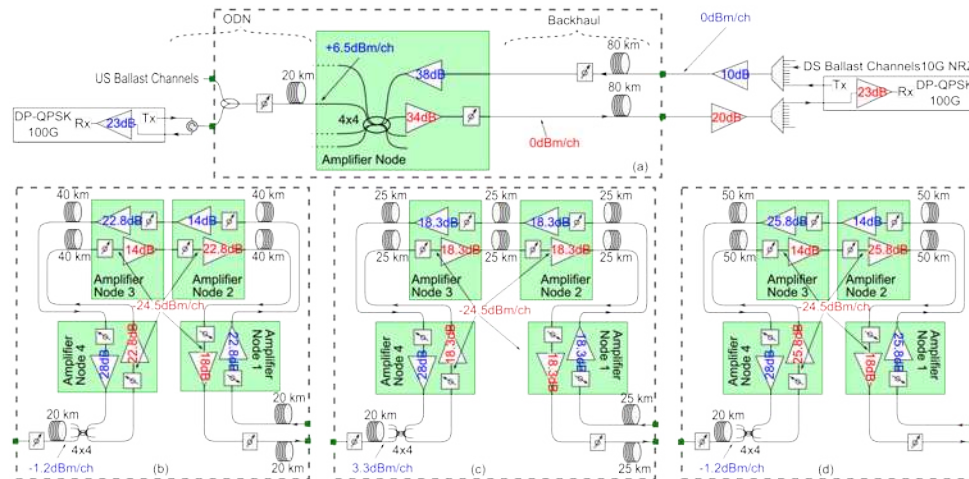

Fig. 5. High level overview of the simulation setups used to model the following LR-PON topologies: (a) tree architecture; (b) open-ring architecture with 2 × 40km links; (c) first alternative open-ring architecture with equal distribution of 25km fiber links; (d) second alternative open-ring architecture with 2 × 50km links.

5.1 Downstream

The design of the downstream link for both tree and open-ring LR-PON architectures was partially modified with respect to the experimental setups to be closer to a system that would be deployed, as shown in Fig. 5. One of the modifications regards the OSNR of the DP-QPSK signal at the output of the CN, which was set to 40dB. For simplicity only ten OOK channels were emulated (five at lower wavelengths and five at higher wavelengths with respect to the 100G channel), as further increasing the number of channels does not have an appreciable impact on performance but affects significantly the simulation time. However, in contrast to the experimental and modeling cases presented in the previous sections, all the channels were 50GHz-spaced as would be the case in a real network scenario and all had the same optical

power. The system performance of the downstream link for all the network architectures illustrated in Fig. 5 was evaluated by measuring the BER of the 100G signal as a function of the 10Gb/s OOK channel power. The BER was also calculated as a function of the power of the 100G signal itself, thus providing a 3D-map with the bounds that determine the three possible operating regimes: SPM-limited; XPM-limited; and OSNR-limited.
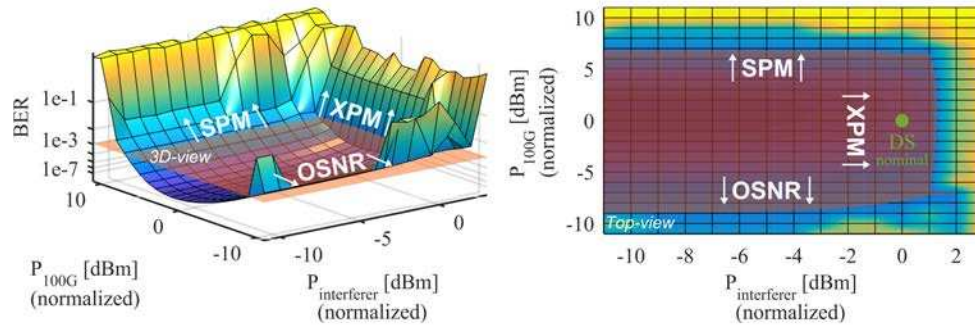

Fig. 6. Downstream BER of the tree architecture as a function of the normalized OOK and 100G signal powers launched from the CN for an ODN loss of 30.5dB. The contour corresponding to the FEC threshold of 1.1E-3 is clearly visible from the top-view.

With regard to the conventional tree architecture, the ODN loss was fixed to 30.5dB, which corresponds to 128 (× 4) split with 20km of distribution fiber. The results are presented in Fig. 6. It should be noted that, for convenience, the powers are normalized to the nominal downstream power at the output of the CN. From the BER values in Fig. 6 it is possible to see that at nominal power there is a robust margin in terms of the 100G channel power of more than 6dB before entering the SPM-limited regime and 7dB before entering the OSNR-limited regime at the FEC threshold. This confirms that launching a DP-QPSK signal of 0dBm from the CN represents a good trade-off between maximum achievable OSNR (and hence maximum ODN loss) and minimum impact from SPM. On the other hand, there is only a modest margin of ~1dB in terms of XPM before exceeding the FEC threshold, and this suggests that the network design could be further improved to increase the reliability and robustness of the system. For example, the launched power of the 10Gb/s OOK channels could be slightly reduced to lower the effect of crosstalk with the 100G signal. While this would result in a reduction of the received power and achievable OSNR for the OOK channels (and hence of the achievable ODN loss), the data reported in [6] shows that it is in fact a valid and feasible solution as the 10Gb/s OOK downstream can support an ODN loss of up to ~36.5dB. This corresponds to a 128 (× 4) split LR-PON with 20km of distribution fiber and a margin of 6dB. Therefore, it is reasonable to reduce this high margin in favor of a more robust 100G downstream link. A good trade-off could be achieved by reducing the 10Gb/s OOK launched power by 3dB approximately. From the results presented so far it is also possible to infer that this network architecture could, in principle, support an even higher number of splits in the downstream direction. Nevertheless, given that the upstream link is eventually limiting the performance to a realistic value of 128 (× 4) splits (see Subsection 5.2) this option is not further discussed in this context.

With regard to the open-ring architecture, the ODN loss was fixed to 27dB, which corresponds to 64 (× 4) split with 20km of distribution fiber. The results are shown in Fig. 7, where the powers are normalized to the nominal downstream power at the output of the CN. From the results of Fig. 7 it is possible to see that at nominal power the system presents a large margin in terms of nonlinearities (the power launched into the various fiber links is ≤0dBm) and a reasonable OSNR margin of 4dB. This further validates the design approach used here. Moreover the results suggest that, in principle, the 100G downstream link is capable of supporting an even higher split-ratio of 128 (× 4) with a small residual OSNR

margin of about 1dB (that could be further improved by launching a higher power from the CN given the great margin in terms of SPM). Once again, since the upstream link is eventually limiting the performance to a realistic value of 64 (× 4) splits (see Subsection 5.2) this option is not further discussed here.
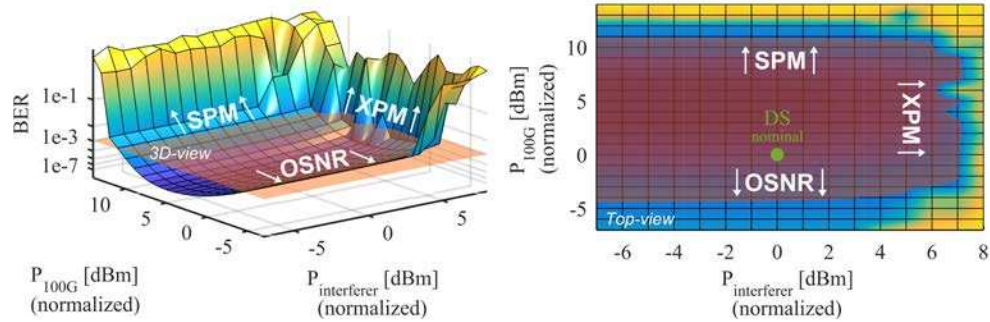

Fig. 7. Downstream BER of the open-ring architecture as a function of the normalized OOK and 100G signal powers. The contour corresponding to the FEC threshold of 1.1E-3 is clearly visible from the top-view.

A detailed analysis was also carried out for the two alternative open-ring topologies of Figs. 5(c) and 5(d) in order to obtain a 3D-map with the bounds that determine the three possible operating regimes for both open-ring designs in the downstream direction. The results, not shown here, are in line with the ones in Fig. 7 and indicate that both architectures can support at least 64 × 4 = 256 with suitable system margins in terms of OSNR as well as nonlinearities. When all intermediate ANs are aggregated this translates in 256 × 4 = 1024 users.

5.2 Upstream

For the upstream design optimization of all the network architectures presented in Fig. 5, the 100G nominal power was actually set in the middle of the PON channels dynamic range with a worst case ODN loss obtained considering 3.5dB of loss for each × 2 split. Once again, the 100G channel was characterized in terms of penalty caused by the nonlinear crosstalk from the two neighboring 10Gb/s OOK PON channels bursting with high power and, in order to simplify the simulation test-bed, the remaining channels were not emulated. We believe that the case analyzed with only the two adjacent high power interfering channels is a realistic worst case taking into account the statistical distribution of the ONUs burst powers and the fact that the adjacent channels cause the major contribution to the non-linear cross-talk. Furthermore, the performance of the DP-QPSK signal was evaluated in the simulations with the 10Gb/s interferers operated in continuous-mode and hence the scaling factor of Eq. (3) was not used in this case. Similarly to the downstream case, by measuring the BER also as a function of the power of the 100G signal itself it was possible to obtain a 3D-map with the bounds that determine the three possible operating regimes.

With regard to the conventional tree architecture, the 100G channel at nominal power experienced an ODN loss of 30.5−6 = 24.5dB and the corresponding results are presented in Fig. 8. It should be noted that, for convenience, the powers are normalized to the nominal upstream power at the input of the EDFA in the AN. From Fig. 8 it is possible to see that at nominal power the 100G upstream link presents large margins both in terms of OSNR as well as nonlinearities. With this specific tree design, only unrealistic operating conditions (i.e. extremely high transmitted powers from the 100G ONU or exceptionally high dynamic ranges for the 10Gb/s PON channels) could cause the 100G BER to exceed the FEC threshold because of nonlinearities. The top-view of Fig. 8 also shows a straight diagonal line that represents the ODN loss of the upstream link. In fact, increasing or decreasing the power of

both 100G signal and 10Gb/s PON channels by the same amount (hence moving the operating point along the straight line) is conceptually like increasing or decreasing the ODN loss. The results show that, assuming a launched power of + 5dBm from the 100G ONU, the link can support an ODN loss of ~30.5dB (i.e. 128 (× 4) split with 20km of fiber) with almost 3dB OSNR margin. This is a further validation of the design approach used here. As a matter of fact, with the help of a higher 100G launched power from the ONU, this margin could be used to further extend the ODN loss. For instance, by launching a 100G power of + 8dBm instead of + 5dBm from the ONU it would be possible to double the split-ratio for the same fiber length (i.e. 34dB ODN loss) and still guarantee ~2dB OSNR margin. As the 10Gb/s PON channels can also support 34dB ODN loss for the worst case soft packet [6], the upstream link could in principle support a 256 (× 4) split LR-PON with 20km of distribution fiber. It should be noted however that this would force the 10Gb/s soft packets to work with an OSNR margin close to zero. Therefore, despite the fact that both down- and up-stream links could in theory support 34dB ODN loss, this represent a rather unrealistic solution as it would reduce the system margins to impractical values. We believe that the best trade-off between maximum achievable number of splits and strong system margins for the conventional tree architecture is represented by the 128 (× 4) split case.
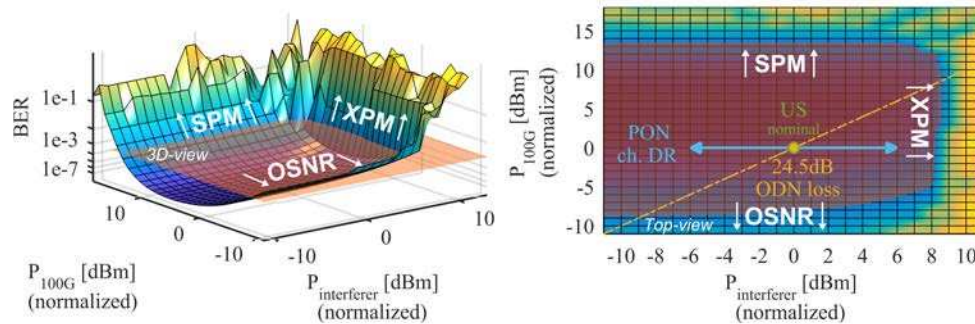

Fig. 8. Upstream BER of the tree architecture as a function of the normalized OOK and 100G signal powers. The contour corresponding to the FEC threshold of 1.1E-3 is clearly visible from the top-view. The straight line visible from the top-view represents the ODN loss.

For all the various open-ring simulation setups illustrated in Fig. 5, the nominal upstream power was centered in the middle of the PON dynamic range with a worst case ODN loss obtained considering 3.5dB of loss for each × 2 split. This means that the 100G channel experienced an ODN loss of 27−4.5 = 22.5dB. The performance characterization was carried out in a similar way to the tree design by defining the bounds that determine the three possible operating regimes. The results relative to the open-ring architecture illustrated in Fig. 5(b) are presented in Fig. 9. It should be noted that, for convenience, the powers are normalized to the nominal upstream power at the input of the first AN EDFA.

From Fig. 9 it is possible to see that, similarly to the open-ring downstream case, at nominal power the system presents a great margin in terms of nonlinearities (the power launched into the various fiber links is ≤−2.5dBm) and a reasonable OSNR margin of approximately 5dB, which further validates the design approach used here. With regard to the maximum achievable number of splits, the results show that in principle the 100G link would be able to support an even higher split-ratio of 128 (× 4) with the help of a higher 100G launched power from the ONU, but eventually the performance is limited by the 10Gb/s PON channels that operate extensively in the OSNR-limited regime with an already tight margin [7]. Therefore, the maximum ODN loss that this architecture can realistically support is limited to 27dB (i.e. 64 (× 4) splits).
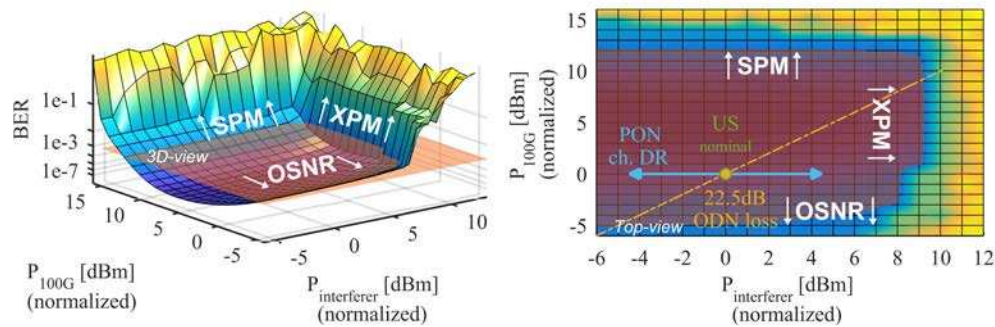
Fig. 9. Upstream BER of the open-ring architecture as a function of the normalized OOK and 100G signal powers. The contour corresponding to the FEC threshold of 1.1E-3 is clearly visible from the top-view. The straight line visible from the top-view represents the ODN loss.

With regard to the two alternative open-ring topologies, a detailed analysis was carried out in order to obtain a 3D-map with the bounds that determine the three possible operating regimes for both designs in the upstream direction. Similarly to the downstream case, the results (not shown here, but in line with Fig. 9) indicate that both architectures can support at least $64 \times 4 = 256$ with suitable system margins in terms of OSNR as well as nonlinearities, which corresponds to $256 \times 4 = 1024$ users when all intermediate ANs are aggregated. These results confirm the flexibility of the open-ring architecture that can be specifically tailored to facilitate the provisioning of users across the most diverse sparsely populated rural areas.

6. Conclusions

The convergence and hence coexistence of heterogeneous service types and modulation formats on a common physical layer is one of the ultimate goals of future access networks. In this converged scenario, the performance of high bandwidth phase modulated signals can be severely affected by nonlinear crosstalk from co-propagating OOK channels. As a consequence, it is fundamental to define the XPM tolerance of such signals in order to establish whether these different services can indeed be supported by a single, common infrastructure. In this paper, the overlay of a 100G DP-QPSK channel in a LR-PON in the presence of co-propagating 10Gb/s OOK neighboring channels has been studied for two different PON architectures, the first one particularly suited for densely populated areas (tree design), and a second one aimed at rural, sparsely populated areas (open-ring). The experimental results relative to the tree design indicated that this type of architecture is able to support $128 \times 4 = 512$ users and a total physical reach of 100km with adequate system margin while also tolerating dynamic-ranges higher than the ones caused by the non-uniform loss (considering standardized values) in the ODN. The experimental results also showed that the novel architecture based on a chain of ANs can support $64 \times 4 = 256$ users per amplifier node (1024 users when all the nodes are aggregated) and a total reach of 120km. Similarly to the tree architecture, the open-ring design also proved to be very robust and capable of tolerating dynamic-ranges higher than the ones caused by the non-uniform loss (considering standardized values) in the ODN. The numerical model developed to reproduce the 100G link full system experimental data for both network architectures shows excellent agreement with the measurements thus validating the modeling approach used here.

The model was then used to predict the system performance and system margins for configurations different from the experimental setup and to carry out design optimization that could in principle lead to even more efficient and robust schemes. With regard to the tree architecture, it was shown that, while the 100G link could in principle support an even higher number of splits in the ODN, the 10Gb/s OOK channels would be forced to work with unrealistic tight system margins making this option impractical. It was confirmed that the best

trade-off between maximum achievable number of splits and robust system margins for the conventional tree architecture is represented by the 128 (× 4) split case. Similar conclusions were drawn also for the open-ring architecture with the configuration shown experimentally, whose 100G link would in principle be able to support twice the number of users, but where the performance is limited by the 10Gb/s OOK channels that operate extensively in the OSNR-limited regime with tight margins. Therefore, the maximum ODN loss that this architecture can realistically support is limited to 27dB (i.e. 64 (× 4) splits). The open-ring case also demonstrated the high flexibility of this novel scheme to different network topologies and customer distributions. By modeling two additional systems with different characteristics in terms of amplifier node locations, it was shown how this design can be used to provision users across geographically diverse rural areas.